

Observation of $B_s^0 \rightarrow D_s^{*-} \pi^+$, $B_s^0 \rightarrow D_s^{(*)-} \rho^+$ Decays and Measurement of $B_s^0 \rightarrow D_s^{*-} \rho^+$ Polarization

R. Louvot,¹⁹ O. Schneider,¹⁹ T. Aushev,^{19,12} K. Arinstein,^{1,33} A. M. Bakich,³⁹ V. Balagura,¹² E. Barberio,²³
 A. Bay,¹⁹ K. Belous,¹¹ M. Bischofberger,²⁵ A. Bondar,^{1,33} A. Bozek,²⁹ M. Bračko,^{21,13} T. E. Browder,⁷
 P. Chang,²⁸ Y. Chao,²⁸ A. Chen,²⁶ K.-F. Chen,²⁸ P. Chen,²⁸ B. G. Cheon,⁶ C.-C. Chiang,²⁸ I.-S. Cho,⁴⁷ Y. Choi,³⁸
 M. Danilov,¹² M. Dash,⁴⁶ A. Drutskoy,³ S. Eidelman,^{1,33} P. Goldenzweig,³ H. Ha,¹⁷ J. Haba,⁸ T. Hara,⁸ Y. Horii,⁴²
 Y. Hoshi,⁴¹ W.-S. Hou,²⁸ Y. B. Hsiung,²⁸ H. J. Hyun,¹⁸ T. Iijima,²⁴ K. Inami,²⁴ R. Itoh,⁸ M. Iwabuchi,⁴⁷
 M. Iwasaki,⁴³ Y. Iwasaki,⁸ N. J. Joshi,⁴⁰ D. H. Kah,¹⁸ J. H. Kang,⁴⁷ P. Kapusta,²⁹ N. Katayama,⁸ T. Kawasaki,³¹
 C. Kiesling,²² H. J. Kim,¹⁸ H. O. Kim,¹⁸ J. H. Kim,¹⁶ M. J. Kim,¹⁸ Y. J. Kim,⁵ K. Kinoshita,³ B. R. Ko,¹⁷
 P. Kodyš,² S. Korpar,^{21,13} P. Krizán,^{20,13} P. Krokovny,⁸ T. Kumita,⁴⁴ Y.-J. Kwon,⁴⁷ S.-H. Kyeong,⁴⁷ J. S. Lange,⁴
 M. J. Lee,³⁷ S.-H. Lee,¹⁷ J. Li,⁷ C. Liu,³⁶ A. Matyja,²⁹ S. McOnie,³⁹ K. Miyabayashi,²⁵ H. Miyata,³¹ Y. Miyazaki,²⁴
 G. B. Mohanty,⁴⁰ M. Nakao,⁸ H. Nakazawa,²⁶ S. Nishida,⁸ K. Nishimura,⁷ O. Nitoh,⁴⁵ T. Ohshima,²⁴ S. Okuno,¹⁴
 S. L. Olsen,^{37,7} P. Pakhlov,¹² G. Pakhlova,¹² H. Palka,²⁹ H. Park,¹⁸ H. K. Park,¹⁸ R. Pestotnik,¹³ M. Petrič,¹³
 L. E. Piilonen,⁴⁶ A. Poluektov,^{1,33} M. Prim,¹⁵ M. Röhrken,¹⁵ S. Ryu,³⁷ H. Sahoo,⁷ Y. Sakai,⁸ C. Schwanda,¹⁰
 A. J. Schwartz,³ K. Senyo,²⁴ M. E. Sevior,²³ M. Shapkin,¹¹ V. Shebalin,^{1,33} C. P. Shen,⁷ J.-G. Shiu,²⁸ J. B. Singh,³⁵
 P. Smerkol,¹³ A. Sokolov,¹¹ S. Stanič,³² M. Starič,¹³ T. Sumiyoshi,⁴⁴ G. N. Taylor,²³ Y. Teramoto,³⁴ K. Trabelsi,⁸
 S. Uehara,⁸ Y. Unno,⁶ S. Uno,⁸ G. Varner,⁷ K. E. Varvell,³⁹ K. Vervink,¹⁹ C. H. Wang,²⁷ M.-Z. Wang,²⁸
 P. Wang,⁹ J. Wicht,⁸ E. Won,¹⁷ B. D. Yabsley,³⁹ Y. Yamashita,³⁰ Z. P. Zhang,³⁶ T. Zivko,¹³ and O. Zyukova^{1,33}

(Belle Collaboration)

¹*Budker Institute of Nuclear Physics, Novosibirsk*

²*Faculty of Mathematics and Physics, Charles University, Prague*

³*University of Cincinnati, Cincinnati, Ohio 45221*

⁴*Justus-Liebig-Universität Gießen, Gießen*

⁵*The Graduate University for Advanced Studies, Hayama*

⁶*Hanyang University, Seoul*

⁷*University of Hawaii, Honolulu, Hawaii 96822*

⁸*High Energy Accelerator Research Organization (KEK), Tsukuba*

⁹*Institute of High Energy Physics, Chinese Academy of Sciences, Beijing*

¹⁰*Institute of High Energy Physics, Vienna*

¹¹*Institute of High Energy Physics, Protvino*

¹²*Institute for Theoretical and Experimental Physics, Moscow*

¹³*J. Stefan Institute, Ljubljana*

¹⁴*Kanagawa University, Yokohama*

¹⁵*Institut für Experimentelle Kernphysik, Karlsruher Institut für Technologie, Karlsruhe*

¹⁶*Korea Institute of Science and Technology Information, Daejeon*

¹⁷*Korea University, Seoul*

¹⁸*Kyungpook National University, Taegu*

¹⁹*École Polytechnique Fédérale de Lausanne (EPFL), Lausanne*

²⁰*Faculty of Mathematics and Physics, University of Ljubljana, Ljubljana*

²¹*University of Maribor, Maribor*

²²*Max-Planck-Institut für Physik, München*

²³*University of Melbourne, School of Physics, Victoria 3010*

²⁴*Nagoya University, Nagoya*

²⁵*Nara Women's University, Nara*

²⁶*National Central University, Chung-li*

²⁷*National United University, Miao Li*

²⁸*Department of Physics, National Taiwan University, Taipei*

²⁹*H. Niewodniczanski Institute of Nuclear Physics, Krakow*

³⁰*Nippon Dental University, Niigata*

³¹*Niigata University, Niigata*

³²*University of Nova Gorica, Nova Gorica*

³³*Novosibirsk State University, Novosibirsk*

³⁴*Osaka City University, Osaka*

³⁵*Panjab University, Chandigarh*

³⁶*University of Science and Technology of China, Hefei*

³⁷*Seoul National University, Seoul*

³⁸*Sungkyunkwan University, Suwon*

³⁹*School of Physics, University of Sydney, NSW 2006*

⁴⁰Tata Institute of Fundamental Research, Mumbai

⁴¹Tohoku Gakuin University, Tagajo

⁴²Tohoku University, Sendai

⁴³Department of Physics, University of Tokyo, Tokyo

⁴⁴Tokyo Metropolitan University, Tokyo

⁴⁵Tokyo University of Agriculture and Technology, Tokyo

⁴⁶IPNAS, Virginia Polytechnic Institute and State University, Blacksburg, Virginia 24061

⁴⁷Yonsei University, Seoul

(Dated: June 21, 2021)

First observations of the $B_s^0 \rightarrow D_s^{*-}\pi^+$, $B_s^0 \rightarrow D_s^-\rho^+$ and $B_s^0 \rightarrow D_s^{*-}\rho^+$ decays are reported together with measurements of their branching fractions: $\mathcal{B}(B_s^0 \rightarrow D_s^{*-}\pi^+) = (2.4_{-0.4}^{+0.5}(\text{stat.}) \pm 0.3(\text{syst.}) \pm 0.4(f_s)) \times 10^{-3}$, $\mathcal{B}(B_s^0 \rightarrow D_s^-\rho^+) = (8.5_{-1.2}^{+1.3}(\text{stat.}) \pm 1.1(\text{syst.}) \pm 1.3(f_s)) \times 10^{-3}$ and $\mathcal{B}(B_s^0 \rightarrow D_s^{*-}\rho^+) = (11.8_{-2.0}^{+2.2}(\text{stat.}) \pm 1.7(\text{syst.}) \pm 1.8(f_s)) \times 10^{-3}$ ($f_s = N_{B_s^{(*)}\bar{B}_s^{(*)}}/N_{b\bar{b}}$). From helicity-angle distributions, we measured the longitudinal polarization fraction in $B_s^0 \rightarrow D_s^{*-}\rho^+$ decays to be $f_L(B_s^0 \rightarrow D_s^{*-}\rho^+) = 1.05_{-0.10}^{+0.08}(\text{stat.})_{-0.04}^{+0.03}(\text{syst.})$. These results are based on a 23.6 fb^{-1} data sample collected at the $\Upsilon(5S)$ resonance with the Belle detector at the KEKB e^+e^- collider.

PACS numbers: 12.39.Hg, 12.39.St, 13.25.Gv, 13.25.Hw, 13.88.+e, 14.40.Nd

The measurement of exclusive $B_s^0 \rightarrow D_s^{(*)-}h^+$ [$h^+ = \pi^+$ or ρ^+] decays is an important milestone in the study of the poorly understood decay processes of the B_s^0 meson. In Refs. [2–5] Belle confirmed the large potential of B factories for B_s^0 investigations due to the low multiplicities of charged and neutral particles and high reconstruction efficiencies. We have now observed three new exclusive B_s^0 modes with relatively large branching fractions and neutral particles such as photons or π^0 's in their final states. The leading amplitude for the four $B_s^0 \rightarrow D_s^{(*)-}\pi^+$ and $B_s^0 \rightarrow D_s^{(*)-}\rho^+$ modes is a $b \rightarrow c$ tree diagram of order λ^2 (in the Wolfenstein parameterization [6] of the CKM quark-mixing matrix [7]) with a spectator s quark. The study of B_s^0 decays provides useful tests of the heavy-quark theories that predict, based on an $SU(3)$ symmetry, similarities between B_s^0 -meson decay modes and their corresponding B^0 -meson counterparts. These include the unitarized quark model [8], the heavy quark effective theory (HQET) [9–12], and a more recent approach based on chiral symmetry [13]. Our B_s^0 branching fraction results can be used to normalize measurements of B_s^0 decays made at hadron collider experiments, where the number of B_s^0 mesons produced has a substantial systematic uncertainty.

The decay $B_s^0 \rightarrow D_s^{*-}h^+$ is mediated by the same tree diagram as $B^0 \rightarrow D^{*-}h^+$, but with a spectator s quark. The contribution of the strongly suppressed W -exchange diagram is expected to be negligibly small. Moreover, the helicity amplitudes in $B \rightarrow VV$ decays can be used to test the factorization hypothesis [12, 14]. The relative strengths of the longitudinal and transverse states can be measured with an angular analysis of the decay products. In the helicity basis, the expected $B_s^0 \rightarrow D_s^{*-}\rho^+$

differential decay width is

$$\frac{d^2\Gamma(B_s^0 \rightarrow D_s^{*-}\rho^+)}{d\cos\theta_{D_s^{*-}}d\cos\theta_{\rho^+}} \propto 4f_L \sin^2\theta_{D_s^{*-}} \cos^2\theta_{\rho^+} + (1 - f_L)(1 + \cos^2\theta_{D_s^{*-}}) \sin^2\theta_{\rho^+}, \quad (1)$$

where $f_L = |H_0|^2/\sum_\lambda |H_\lambda|^2$ is the longitudinal polarization fraction, H_λ ($\lambda = \pm 1, 0$) are the helicity amplitudes, and $\theta_{D_s^{*-}}$ (θ_{ρ^+}) is the helicity angle of the D_s^{*-} (ρ^+) defined as the supplement of the angle between the B_s^0 and the D_s^- (π^+) momenta in the D_s^{*-} (ρ^+) frame.

Here we report measurements performed with fully reconstructed $B_s^0 \rightarrow D_s^{*-}\pi^+$, $B_s^0 \rightarrow D_s^-\rho^+$ and $B_s^0 \rightarrow D_s^{*-}\rho^+$ decays in a data set corresponding to an integrated luminosity of $L_{\text{int}} = (23.6 \pm 0.3) \text{ fb}^{-1}$ collected with the Belle detector at the KEKB asymmetric-energy (3.6 GeV on 8.2 GeV) e^+e^- collider [15] operated at the $\Upsilon(5S)$ resonance ($\sqrt{s} = 10867.0 \pm 1.0 \text{ MeV}$ [5]). The total $b\bar{b}$ cross section at the $\Upsilon(5S)$ energy has been measured to be $\sigma_{b\bar{b}}^{\Upsilon(5S)} = (0.302 \pm 0.014) \text{ nb}$ [2, 16]. Three B_s^0 production modes are kinematically allowed at the $\Upsilon(5S)$: $B_s^*\bar{B}_s^*$, $B_s^*\bar{B}_s^0 + B_s^0\bar{B}_s^*$, and $B_s^0\bar{B}_s^0$. The B_s^* decays to B_s^0 , emitting a photon with energy $E_\gamma \sim 50 \text{ MeV}$. The fraction of $b\bar{b}$ events containing a $B_s^{(*)}\bar{B}_s^{(*)}$ pair has been measured to be $f_s = N_{B_s^{(*)}\bar{B}_s^{(*)}}/N_{b\bar{b}} = (19.3 \pm 2.9)\%$ [17]. The fraction of $B_s^{(*)}\bar{B}_s^{(*)}$ events containing a $B_s^*\bar{B}_s^*$ pair is predominant and has been measured with $B_s^0 \rightarrow D_s^-\pi^+$ events to be $f_{B_s^*\bar{B}_s^*} = (90.1_{-4.0}^{+3.8} \pm 0.2)\%$ [5]. The number of B_s^0 mesons produced in the dominant $B_s^*\bar{B}_s^*$ production mode is thus $N_{B_s^0} = 2 \times L_{\text{int}} \times \sigma_{b\bar{b}}^{\Upsilon(5S)} \times f_s \times f_{B_s^*\bar{B}_s^*} = (2.48 \pm 0.41) \times 10^6$.

The Belle detector is a large-solid-angle magnetic spectrometer that consists of a silicon vertex detector, a central drift chamber (CDC), an array of aerogel threshold Cherenkov counters (ACC), a barrel-like arrangement of time-of-flight scintillation counters (TOF), and an elec-

tromagnetic calorimeter comprised of CsI(Tl) crystals (ECL) located inside a superconducting solenoid coil that provides a 1.5 T magnetic field. An iron flux-return located outside of the coil is instrumented to detect K_L^0 and to identify muons. The detector is described in detail elsewhere [18].

Reconstructed charged tracks are required to have a maximum impact parameter with respect to the nominal interaction point of 0.5 cm in the radial direction and 3 cm in the beam-axis direction. A likelihood ratio $\mathcal{R}_{K/\pi} = \mathcal{L}_K/(\mathcal{L}_\pi + \mathcal{L}_K)$ is constructed using ACC, TOF and CDC (ionization energy loss) measurements. A track is identified as a charged pion if $\mathcal{R}_{K/\pi} < 0.6$ or as a charged kaon otherwise. With this selection, the momentum-averaged identification efficiency for pions (kaons) is about 91% (86%), while the momentum-averaged rate of kaons (pions) identified as pions (kaons) is about 9% (14%).

Photons are reconstructed using ECL energy clusters within the polar angle acceptance 17° to 150° that are not associated with a charged track and that have an energy deposit larger than 50 MeV. A photon candidate is retained only if the ratio of the energy deposited in the array of the central 3×3 cells is more than 85% of that in the array of 5×5 cells. Neutral pions are reconstructed via the $\pi^0 \rightarrow \gamma\gamma$ decay with photon pairs having an invariant mass within ± 13 MeV/ c^2 of the π^0 mass. A mass-constrained fit is then applied to the π^0 candidates.

Neutral kaons are reconstructed via the decay $K_S^0 \rightarrow \pi^+\pi^-$ with no $\mathcal{R}_{K/\pi}$ requirements for the two charged pions. The K_S^0 candidates are required to have an invariant mass within ± 7.5 MeV/ c^2 of the K_S^0 mass. Requirements are applied on the K_S^0 vertex displacement from the interaction point (IP) and on the difference between the K_S^0 flight directions obtained from the K_S^0 momentum and from the decay vertex and IP. The criteria are described in detail elsewhere [19]. The $K^{*0}(\phi, \rho^+)$ candidates are reconstructed via the decay $K^{*0} \rightarrow K^+\pi^-$ ($\phi \rightarrow K^+K^-$, $\rho^+ \rightarrow \pi^+\pi^0$) with an invariant mass within ± 50 MeV/ c^2 (± 12 MeV/ c^2 , ± 100 MeV/ c^2) of their nominal values. Candidates for D_s^- are reconstructed in the three modes $D_s^- \rightarrow \phi\pi^-$, $D_s^- \rightarrow K^{*0}K^-$, and $D_s^- \rightarrow K_S^0K^-$ and are required to have a mass within ± 10 MeV/ c^2 of the D_s^- mass. The D_s^{*-} candidates are reconstructed via the decay $D_s^{*-} \rightarrow D_s^-\gamma$ by adding a photon candidate to a D_s^- candidate. The $D_s^-\gamma$ pair is required to have a mass difference $m(D_s^-\gamma) - m(D_s^-)$ within ± 13 MeV/ c^2 of the $D_s^{*-} - D_s^-$ mass difference. All mass values are those reported in Ref. [17], and the applied mass windows correspond to $\pm(3-4)\sigma$ around these values; the mass resolution, σ , is obtained from MC signal simulations.

The $B_s^0 \rightarrow D_s^{*-}\pi^+$ and $B_s^0 \rightarrow D_s^-\rho^+$ candidates are reconstructed using two variables: the beam-energy-constrained mass of the B_s^0 candidate $M_{bc} =$

$\sqrt{E_b^{*2} - \vec{p}_{B_s^0}^{*2}}$, and the energy difference $\Delta E = E_{B_s^0}^* - E_b^*$, where $(E_{B_s^0}^*, \vec{p}_{B_s^0}^*)$ is the four-momentum of the B_s^0 candidate and E_b^* is the beam energy, both expressed in the center-of-mass frame. The two angles $\theta_{D_s^{*-}}$ and θ_{ρ^+} are used as additional observables for the $B_s^0 \rightarrow D_s^{*-}\rho^+$ candidate. We select candidates with $M_{bc} > 5.3$ GeV/ c^2 and -0.3 GeV $< \Delta E < 0.4$ GeV.

Further selection criteria are developed using Monte Carlo (MC) samples based on the EvtGen [20] event generator and the GEANT [21] full-detector simulation. The most significant source of background is continuum processes, $e^+e^- \rightarrow q\bar{q}$ ($q = u, d, s, c$). In addition, peaking backgrounds can arise from specific B_s^0 decays. Using a MC sample of $e^+e^- \rightarrow B_s^{(*)}\bar{B}_s^{(*)}$ events corresponding to three times the integrated luminosity, we find that $B_s^0 \rightarrow D_s^-\pi^+$ and $B_s^0 \rightarrow D_s^-\rho^+$ events make a significant contribution to the background in the $B_s^0 \rightarrow D_s^{*-}\pi^+$ analysis. However, they are well separated from the signal in the ΔE distribution. If a $B_s^0 \rightarrow D_s^-\pi^+$ decay is combined with an extra photon, the energy is larger than the signal; the four charged tracks of a $B_s^0 \rightarrow D_s^-\rho^+$ event can be selected with an additional photon giving a B_s^0 candidate with a smaller energy. Similarly, $B_s^0 \rightarrow D_s^{*-}\rho^+$ decays give a significant contribution to the $B_s^0 \rightarrow D_s^-\rho^+$ analysis at lower energies. For the $B_s^0 \rightarrow D_s^{*-}\rho^+$ analysis, there is no significant peaking background. MC studies show that, for the three modes, all the other background sources (mainly B^0 and B^+ events) are smooth and small enough to be well described by the same shape that is used for the continuum. The contribution of non-resonant $B_s^0 \rightarrow D_s^{(*)-}\pi^+\pi^0$ decays is studied by relaxing the $(\pi^+\pi^0)$ mass ($M_{\pi\pi}$) requirement and doing a two-dimensional fit in M_{bc} and ΔE (see below). The signal $M_{\pi\pi}$ distribution is then obtained using the $_s$ Plot method [22]. The resulting $M_{\pi\pi}$ spectrum shows no indication of $B_s^0 \rightarrow D_s^{(*)-}\pi^+\pi^0$ decays (consistent with results for $B^0 \rightarrow D^{(*)+}\pi^0\pi^-$ [23]), and we neglect this component in our fit.

To improve signal significance, criteria for each of the three B_s^0 modes are chosen to maximize $N_{\text{sig}}/\sqrt{N_{\text{sig}} + N_{\text{bkg}}^{q\bar{q}} + N_{\text{bkg}}^{\text{peak}}}$, evaluated in the $\pm 2.5\sigma$ $B_s^*\bar{B}_s^*$ signal region in the $(M_{bc}, \Delta E)$ plane. The expected continuum background, $N_{\text{bkg}}^{q\bar{q}}$, is estimated using MC-generated continuum events corresponding to three times the data. The expected signal, N_{sig} , and peaking background, $N_{\text{bkg}}^{\text{peak}}$, are obtained assuming $\mathcal{B}(B_s^0 \rightarrow D_s^-\pi^+) = \mathcal{B}(B_s^0 \rightarrow D_s^{*-}\pi^+) = 3.3 \times 10^{-3}$ [17] and $\mathcal{B}(B_s^0 \rightarrow D_s^-\rho^+) = \mathcal{B}(B_s^0 \rightarrow D_s^{*-}\rho^+) = 7.0 \times 10^{-3}$ [9]. The efficiencies of exclusive B_s^0 decays are determined using MC simulations.

To suppress the continuum background, we use the ratio of the second and zeroth Fox-Wolfram moments [24], R_2 . This variable has a broad distribution between zero and one for jet-like continuum events and

is concentrated in the range below 0.5 for the more spherical signal events. This property allows an efficient continuum reduction with a low systematic uncertainty ($\sim 2\%$). Candidates for $B_s^0 \rightarrow D_s^{*-}\pi^+$ ($B_s^0 \rightarrow D_s^-\rho^+$ and $B_s^0 \rightarrow D_s^{*-}\rho^+$) are required to have $R_2 < 0.5$ (< 0.35). This selection rejects 40% (69%, 64%) of the background while retaining 93% (82%, 86%) of the $B_s^0 \rightarrow D_s^{*-}\pi^+$ ($B_s^0 \rightarrow D_s^-\rho^+$, $B_s^0 \rightarrow D_s^{*-}\rho^+$) signal.

After the event selection described above, about 15%, 15%, and 28% of $D_s^{*-}\pi^+$, $D_s^-\rho^+$ and $D_s^{*-}\rho^+$ candidate events, respectively, have multiple candidates. We select one candidate per event according to the following criteria. The D_s^+ with the mass closest to the nominal value is preferred. The D_s^{*+} formed with the preferred D_s^+ and with the mass difference $m(D_s^*) - m(D_s)$ closest to the nominal value is preferred. The $B_s^0 \rightarrow D_s^{*-}\pi^+$ candidate with the preferred D_s^{*-} and the π^+ with the best $\mathcal{R}_{K/\pi}$ is retained. The preferred ρ^+ is the one with the π^0 mass (before the mass-constrained fit) closest to the nominal value and the π^+ with the best $\mathcal{R}_{K/\pi}$. The $B_s^0 \rightarrow D_s^-\rho^+$ ($B_s^0 \rightarrow D_s^{*-}\rho^+$) candidate with the preferred D_s^- (D_s^{*-}) and the preferred ρ^+ is retained. After this selection, in MC signal simulations, 76%, 68% and 51% (64%) of the selected $B_s^0 \rightarrow D_s^{*-}\pi^+$, $B_s^0 \rightarrow D_s^-\rho^+$ and longitudinally (transversally) polarized $B_s^0 \rightarrow D_s^{*-}\rho^+$ candidates are correctly reconstructed.

The $B_s^0 \rightarrow D_s^{*-}\pi^+$ and $B_s^0 \rightarrow D_s^-\rho^+$ signals are extracted from a two-dimensional unbinned extended maximum likelihood fit [25] in M_{bc} and ΔE . The three decays of the $\Upsilon(5S)$ ($B_s^*\bar{B}_s^*$, $B_s^*\bar{B}_s^0 + B_s^0\bar{B}_s^*$ and $B_s^0\bar{B}_s^0$) are considered. Each signal probability density function (PDF) is described with sums of Gaussian or so-called ‘‘Novosibirsk functions’’ [26]; the latter function is used to describe the distribution if it is asymmetrical around its central value. Each signal PDF is composed of two components with their respective proportions fixed, representing the correctly and the incorrectly reconstructed candidates. In a simulated signal event, a candidate is correctly (incorrectly) reconstructed when the selected decay products do (do not) match the true combination. The fractions of correctly reconstructed candidates are fixed from MC samples and their uncertainties are included in the systematic error. The M_{bc} and ΔE resolutions for $B_s^0 \rightarrow D_s^{*-}\pi^+$ ($B_s^0 \rightarrow D_s^-\rho^+$ and $B_s^0 \rightarrow D_s^{*-}\rho^+$) are calibrated by a multiplying factor measured with the $B_s^0 \rightarrow D_s^-\pi^+$ [$B^0 \rightarrow D^{*-}\rho^+$] signal. The mean values of M_{bc} and ΔE for the three B_s^0 production modes (6 parameters) are related to two floating parameters corresponding to the B_s^0 and B_s^* meson masses [27]. The peaking background PDFs are analytically defined and fixed from specific MC samples. The continuum (together with possible B^+ and B^0 background) is modeled with an ARGUS function [28] for M_{bc} and a linear function for ΔE . The endpoint of the ARGUS function is fixed to the beam energy, while the two other parameters are left free. All the yields can float.

TABLE I: Total efficiencies (ε), signal yields (N_S) with statistical errors, and significance (S) including systematic uncertainties, for the three measured modes.

Mode	Prod. mode	ε (%)	N_S	S
$B_s^0 \rightarrow D_s^{*-}\pi^+$	$B_s^*\bar{B}_s^*$	9.13	$53.4_{-9.4}^{+10.3}$	7.1σ
	$B_s^*\bar{B}_s^0 + B_s^0\bar{B}_s^*$	–	$-1.9_{-2.9}^{+4.0}$	–
	$B_s^0\bar{B}_s^0$	–	$2.9_{-3.0}^{+3.9}$	–
$B_s^0 \rightarrow D_s^-\rho^+$	$B_s^*\bar{B}_s^*$	4.40	$92.2_{-13.2}^{+14.2}$	8.2σ
	$B_s^*\bar{B}_s^0 + B_s^0\bar{B}_s^*$	–	$-4.0_{-3.7}^{+5.2}$	–
	$B_s^0\bar{B}_s^0$	–	$-3.0_{-4.0}^{+5.7}$	–
$B_s^0 \rightarrow D_s^{*-}\rho^+$	$B_s^*\bar{B}_s^*$	–	$77.7_{-13.3}^{+14.6}$	7.4σ
	Longitudinal component	2.66	$81.3_{-14.9}^{+16.0}$	–
	Transverse component	2.68	$-3.5_{-6.1}^{+8.0}$	–

For the $B_s^0 \rightarrow D_s^{*-}\rho^+$ candidates, we perform a four-dimensional fit using the two observables $\cos\theta_{D_s^{*-}}$ and $\cos\theta_{\rho^+}$ in addition to M_{bc} and ΔE . Only the main B_s^0 production mode is considered ($B_s^*\bar{B}_s^*$), and three components are used in the likelihood: the transverse and longitudinal signals, and the background. We define the PDF for M_{bc} and ΔE in the same way as described above, while the angular distributions are analytically described with polynomials of order up to five. The shape parameters are floated for the background PDF but are fixed for the two signal PDFs.

The fitted signal yields are listed in Table I, while Figs. 1 and 2 show the observed distributions in the $B_s^*\bar{B}_s^*$ signal region with the projections of the fit result. The significance is defined by $S = \sqrt{2 \ln(\mathcal{L}_{\max}/\mathcal{L}_0)}$, where \mathcal{L}_{\max} (\mathcal{L}_0) is the value at the maximum (with the corresponding yield set to zero) of the likelihood function convolved with a Gaussian distribution that represents the systematic errors of the yield. The linearity of the floating parameters in the region near the results has been extensively checked with MC simulations, as well as the statistical uncertainty of $f_L(B_s^0 \rightarrow D_s^{*-}\rho^+)$, which lies near the limit of the physically allowed range (0 – 1).

The dominance of the $\Upsilon(5S) \rightarrow B_s^*\bar{B}_s^*$ mode is confirmed. For better precision, we therefore extract the branching fractions (BF) using only the yields in this mode. Table II shows the values obtained with the relations $\mathcal{B} = N_S/(N_{B_s^0} \times \varepsilon)$, for the $B_s^0 \rightarrow D_s^{*-}\pi^+$ and $B_s^0 \rightarrow D_s^-\rho^+$ modes. The values for $\mathcal{B}(B_s^0 \rightarrow D_s^{*-}\rho^+)$ and $f_L = 1.05_{-0.10}^{+0.08}(\text{stat.})_{-0.04}^{+0.03}(\text{syst.})$ are obtained by floating these two parameters in a fit where the longitudinal (transverse) yield is replaced by the relation $N_{B_s^0} \times \mathcal{B} \times f_L \times \varepsilon_L$ ($N_{B_s^0} \times \mathcal{B} \times (1 - f_L) \times \varepsilon_T$), with $N_{B_s^0}$, ε_T and ε_L being fixed. Since the transverse yield fluctuated to a negative central value, $f_L > 1$. The common systematic uncertainties on the BF are due to the errors on the integrated luminosity (1.3%), $\sigma_{bb}^{\Upsilon(5S)}$ (4.6%), f_s (15.0%), $f_{B_s^*\bar{B}_s^*}$ (4.3%), the D_s^- BF (6.4%), the R_2 cut

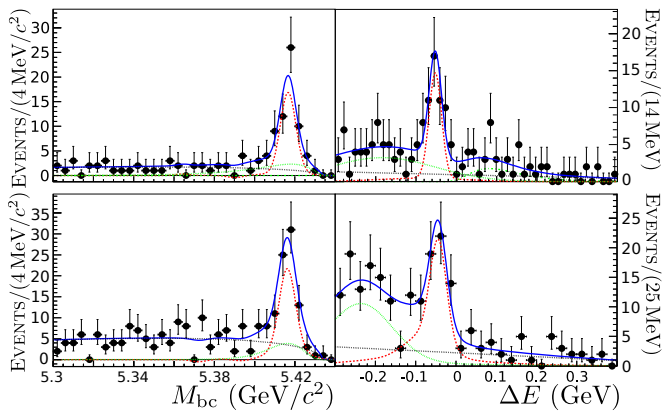


FIG. 1: Left (right): M_{bc} (ΔE) distributions for the $B_s^0 \rightarrow D_s^{*-} \pi^+$ (top) and $B_s^0 \rightarrow D_s^{*-} \rho^+$ (bottom) candidates with ΔE (M_{bc}) restricted to the $\pm 2.5\sigma$ $B_s^* \bar{B}_s^*$ signal region. The blue solid curve is the total PDF, while the green (black) dotted curve is the peaking (continuum) background and the red dashed curve is the signal.

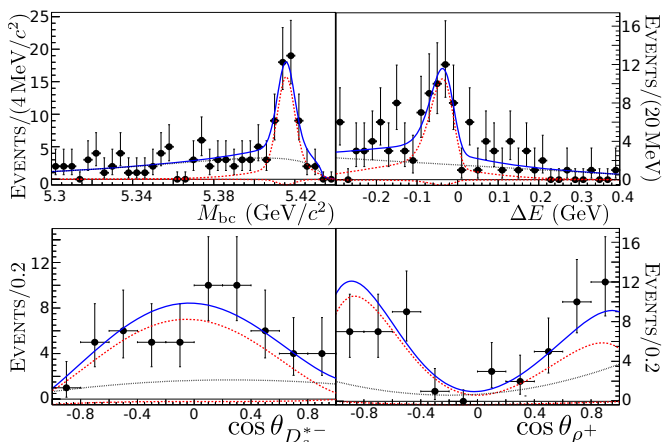


FIG. 2: Distributions for the $B_s^0 \rightarrow D_s^{*-} \rho^+$ candidates. Top: M_{bc} and ΔE distributions, as in Fig. 1. Bottom: helicity distributions of the D_s^{*-} (left) and ρ^+ (right) with M_{bc} and ΔE restricted to the $B_s^* \bar{B}_s^*$ kinematic region. The components of the total PDF (blue solid line) are shown separately: the black-dotted curve is the background and the two red-dashed curve are the signal. The large (small) signal shape corresponds to the longitudinal (transverse) component.

(2.0%), the tracking efficiency (4.0%) and the charged-particle identification (5.4%). In addition, uncertainties due to the MC statistics (1.6%, 2.3%, 1.5%), the neutral-particle identification (8.8%, 5.4%, 8.8%) and the PDF shapes (4.6%, 4.7%, 4.3%) depend on the ($B_s^0 \rightarrow D_s^{*-} \pi^+$, $B_s^0 \rightarrow D_s^{*-} \rho^+$, $B_s^0 \rightarrow D_s^{*-} \rho^+$) mode. The systematic errors on f_L are due to the uncertainties in PDF shapes.

Our values for the BF are in good agreement with predictions based on HQET and the factorization approximation [11]. The large value of $f_L(B_s^0 \rightarrow D_s^{*-} \rho^+)$ is consistent with the value measured for $B^0 \rightarrow D^{*-} \rho$ decays [29] and with the predictions of Refs. [9, 30].

TABLE II: Top: measured BF values with statistical, systematic (without f_s) and f_s uncertainties, and HQET predictions from the factorization hypothesis [11]. Bottom: BF ratios where several systematic uncertainties cancel out. We use our previous measurement of $\mathcal{B}(B_s^0 \rightarrow D_s^- \pi^+)$ [5].

Mode	\mathcal{B} (10^{-3})	HQET (10^{-3})
$B_s^0 \rightarrow D_s^{*-} \pi^+$	$2.4^{+0.5}_{-0.4} \pm 0.3 \pm 0.4$	2.8
$B_s^0 \rightarrow D_s^- \rho^+$	$8.5^{+1.3}_{-1.2} \pm 1.1 \pm 1.3$	7.5
$B_s^0 \rightarrow D_s^{*-} \rho^+$	$11.8^{+2.2}_{-2.0} \pm 1.7 \pm 1.8$	8.9
Ratios		
$\mathcal{B}(B_s^0 \rightarrow D_s^{*-} \pi^+)/\mathcal{B}(B_s^0 \rightarrow D_s^- \pi^+) = 0.65^{+0.15}_{-0.13} \pm 0.07$		
$\mathcal{B}(B_s^0 \rightarrow D_s^- \rho^+)/\mathcal{B}(B_s^0 \rightarrow D_s^- \pi^+) = 2.3 \pm 0.4 \pm 0.2$		
$\mathcal{B}(B_s^0 \rightarrow D_s^{*-} \rho^+)/\mathcal{B}(B_s^0 \rightarrow D_s^- \pi^+) = 3.2 \pm 0.6 \pm 0.3$		
$\mathcal{B}(B_s^0 \rightarrow D_s^{*-} \rho^+)/\mathcal{B}(B_s^0 \rightarrow D_s^- \rho^+) = 1.4 \pm 0.3 \pm 0.1$		

In summary, we report the first observation of three CKM-favored exclusive B_s^0 decay modes, we extract their branching fractions, and, for $B_s^0 \rightarrow D_s^{*-} \rho^+$, we measure the longitudinal polarization fraction. Our results are consistent with theoretical predictions based on HQET [11] and are similar to analogous B^0 decay branching fractions. The dominance of the unexpectedly large $\Upsilon(5S) \rightarrow B_s^* \bar{B}_s^*$ mode [5] is confirmed.

We thank the KEKB group for excellent operation of the accelerator, the KEK cryogenics group for efficient solenoid operations, and the KEK computer group and the NII for valuable computing and SINET3 network support. We acknowledge support from MEXT, JSPS and Nagoya's TLPRC (Japan); ARC and DIISR (Australia); NSFC (China); MSMT (Czechia); DST (India); MEST, NRF, NSDC of KISTI, and WCU (Korea); MNiSW (Poland); MES and RFAAE (Russia); ARRS (Slovenia); SNSF (Switzerland); NSC and MOE (Taiwan); and DOE (USA).

- [1] Unless specified otherwise, charge-conjugated modes are implied throughout.
- [2] A. Drutskoy *et al.* (Belle Collaboration), Phys. Rev. Lett. **98**, 052001 (2007).
- [3] A. Drutskoy *et al.* (Belle Collaboration), Phys. Rev. D **76**, 012002 (2007).
- [4] J. Wicht *et al.* (Belle Collaboration), Phys. Rev. Lett. **100**, 121801 (2008).
- [5] R. Louvot *et al.* (Belle Collaboration), Phys. Rev. Lett. **102**, 021801 (2009).
- [6] L. Wolfenstein, Phys. Rev. Lett. **51**, 1945 (1983).
- [7] M. Kobayashi and T. Maskawa, Prog. Theor. Phys. **49**, 652 (1973); N. Cabibbo, Phys. Rev. Lett. **10**, 531 (1963).
- [8] N.A. Törnqvist, Phys. Rev. Lett. **53**, 878 (1984).
- [9] J.L. Rosner, Phys. Rev. D **42**, 3732 (1990).
- [10] B. Block and M. Shifman, Nucl. Phys. B **389**, 534 (1993).
- [11] A. Deandrea *et al.*, Phys. Lett. B **318**, 549 (1993).

- [12] T. Mannel, W. Roberts and Z. Ryzak, Phys. Lett. B **259**, 359 (1991).
- [13] W. Bardeen, E. Eichten and C. Hill, Phys. Rev. D **68**, 054024 (2003).
- [14] J.G. Körner and G.R. Goldstein, Phys. Lett. B **89**, 105 (1979).
- [15] S. Kurokawa and E. Kikutani, Nucl. Instrum. Methods Phys. Res., Sect. A **499**, 1 (2003), and other articles included in this Volume.
- [16] G.S. Huang *et al.* (CLEO Collaboration), Phys. Rev. D **75**, 012002 (2007).
- [17] C. Amsler *et al.* (Particle Data Group), Phys. Lett. B **667**, 1 (2008).
- [18] A. Abashian *et al.* (Belle Collaboration), Nucl. Instrum. Methods Phys. Res., Sect. A **479**, 117 (2002).
- [19] F. Fang, Ph.D. thesis, University of Hawaii (2003).
- [20] D.J. Lange, Nucl. Instrum. Methods Phys. Res., Sect. A **462**, 152 (2001).
- [21] CERN Application Software Group (1993), CERN Program Library, W5013.
- [22] M. Pivk and F.R. Le Diberder, Nucl. Instrum. Methods A **555**, 356 (2005).
- [23] M.S. Alam *et al.* (CLEO Collaboration), Phys. Rev. D **50**, 43 (1994).
- [24] G.C. Fox and S. Wolfram, Phys. Rev. Lett. **41**, 1581 (1978).
- [25] R. Barlow, Nucl. Instrum. Methods Phys. Res., Sect. A **297**, 496 (1990).
- [26] The Novosibirsk function is defined as $f(x) = \exp[-\frac{1}{2}(\ln^2(1 + \Lambda(x - x_0))/\tau^2 + \tau^2)]$ with $\Lambda = \sinh(\tau\sqrt{\ln 4})/(\sigma\sqrt{\ln 4})$. The parameters represent the mean (x_0), the width (σ) and the tail asymmetry (τ).
- [27] See Table I of Ref. [5] for the detailed parameterization.
- [28] H. Albrecht *et al.* (ARGUS Collaboration), Phys. Lett. B **185**, 218 (1987).
- [29] S.E. Csorna *et al.* (CLEO Collaboration), Phys. Rev. D **67**, 112002 (2003).
- [30] A. Ali *et al.*, Z. Phys. C **1**, 269 (1979).